The Surface-Wind Response to Transient Mesoscale Pressure Fields Associated with Squall Lines

MICHAEL D. VESCIO* AND RICHARD H. JOHNSON

Atmospheric Science Department, Colorado State University, Fort Collins, Colorado

(Manuscript received 23 July 1991, in final form 9 December 1991)

ABSTRACT

The two most prominent surface pressure features associated with squall lines are 1) a surface mesohigh, centered within the heavy-rain region, and 2) a wake low, located at the back edge of the trailing area of light rainfall. The surface flow near these features is often highly unbalanced due to propagation and transience of the pressure fields. Centers of surface divergence and convergence are typically displaced rearward of the mesohigh and wake-low axes, respectively.

In an attempt to explain the basic mesoscale characteristics of the surface flow in the vicinity of squall lines, a simplified model of a propagating mesohigh–wake-low couplet is developed using a one-dimensional slab model of the boundary layer. The component of the flow normal to the squall line is predicted, with advective and frictional effects included but the Coriolis force neglected. Model results are compared to the observed airflow near the mesohigh and wake low associated with an intense squall line that moved through Oklahoma and Kansas on 10–11 June 1985.

The primary mesoscale features of the surface flow associated with squall lines are explained by the model. Displacement of the divergence and convergence axes to the rear of the mesohigh and wake-low axes is a result of propagation of the system. Strong winds are found out ahead of the mesohigh when the phase speed of the pressure wave matches the air-parcel velocities. This effect, along with the vertical transport of momentum by the convective line, can cause surging of the winds along the gust front. Strong surface convergence can occur behind the wake low even for weak pressure disturbances, which may account for the generation of new convection to the rear of some squall lines. In addition, as a result of reduced friction, strong and damaging winds may develop in the vicinity of wake lows that pass over open-water areas. Some squall lines possess very intense pressure gradients between the mesohigh and wake low (on occasion equivalent to that in the eyewall of a moderate hurricane); however, hurricane-force winds normally do not develop because air parcels do not stay in this gradient long enough to achieve extreme velocities.

1. Introduction

Organized mesoscale convective systems (MCSs), such as squall lines, frequently have distinct surface pressure features associated with them. Mesohighs occur in the region of heavy precipitation, and mesolows can develop in advance of and behind the storms. In some instances, intense pressure gradients can develop, with pressure changes as much as 2–6 mb or more in as little as 5 min occurring at a point (Brunk 1949; Williams 1948, 1953; Stumpf et al. 1991). The mesohigh is primarily a consequence of evaporative cooling within the heavy-rain area, whereas the wake low is a result of strong subsidence within the *rear-inflow jet* (Smull and Houze 1987) behind the squall-line system (Johnson and Hamilton 1988).

Typical surface pressure features associated with a squall line possessing a trailing stratiform region are shown in Fig. 1 [revised from Johnson and Hamilton (1988) based on the results of the present study]. This schematic illustrates the highly ageostrophic character of the surface flow in these systems (Brunk 1949, 1953; Williams 1954; Fujita 1955). The instantaneous ground-relative airflow is directed forward through the mesohigh and rearward through the wake low. A difluence axis is located behind the high center with confluence occurring near the back edge of the wake low. The unbalanced flow near these pressure fields results from their transient nature, as shown by Mahrt (1974) and Garratt and Physick (1983).

A one-dimensional (1D) slab model was developed by Garratt and Physick (1983) to investigate the wind response to changing pressure fields occurring with convective systems over southern Australia. The boundary layer was treated in a bulk sense with friction represented by a drag formulation. The momentum

* Current affiliation: National Weather Service, Raleigh, NC 27623-0337.

Corresponding author address: Dr. Richard H. Johnson, Colorado State University, Department of Atmospheric Science, Fort Collins, CO 80523.

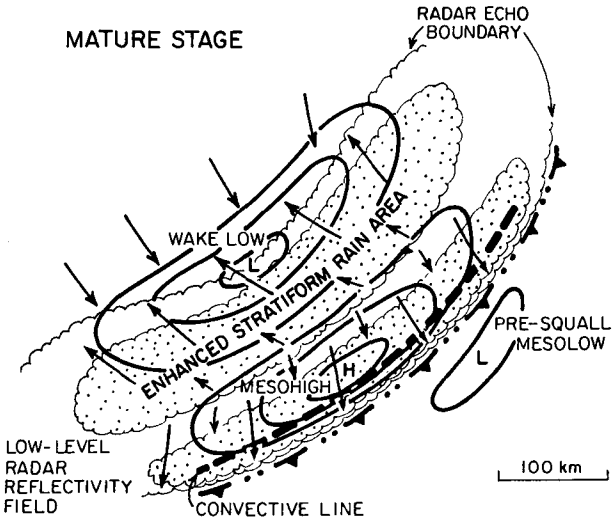

FIG. 1. Schematic low-level reflectivity pattern, surface pressure, and ground-relative surface-wind distributions during a squall-line mature stage (revised from Johnson and Hamilton 1988).

equation for the component of the flow normal to the long axis of the pressure field was solved with Coriolis effects included. Useful analytical solutions were obtained when the nonlinear effects of advection were omitted.

In this study, we modify the model of Garratt and Physick (1983) to include nonlinear advective effects, which have been determined to be important in our investigation. A similar conclusion has been drawn by Green (1989) in her analysis of the surface flow field for an MCS that occurred during the OK PRE-STORM [Oklahoma–Kansas Preliminary Regional Experiment for STORM (Stormscale Operational and Research Meteorology)-Central] on 3–4 May 1985. Since the evolution over just a few hours is considered, Coriolis effects are neglected. The squall-line pressure field is represented by an amplifying, then steady, sine wave that propagates at a constant phase speed. Air-parcel trajectories through the wave are evaluated to help explain the airflow pattern in Fig. 1. Sensitivity to surface friction and momentum transfer at the boundary-layer top by convection are also investigated. Specific application is given to an intense squall line having a trailing stratiform region that moved through the OK PRE-STORM data network on 10–11 June 1985.

Before proceeding further, it is appropriate to comment on the philosophy behind the simple modeling approach adopted in this paper. One alternative would be to employ a nonhydrostatic mesoscale model of the squall line and diagnose the results relative to the processes discussed here. The latter approach, though not utilized in this study, is an option that should provide valuable information concerning the dynamics of the pressure systems (e.g., the role of evaporation in producing the mesohigh, the effects of vertical transport of momentum, and other processes affecting the surface wind field). In our investigation, however, we use a simple model patterned after that of Garratt and Physick (1983) to gain insight into the fundamental physical processes, which can be further explored by more sophisticated models.

2. Observations of the 10–11 June MCS

A number of studies have examined the 10–11 June 1985 OK PRE-STORM squall line. Johnson and Hamilton (1988) and Rutledge et al. (1988) discussed the life cycle of this MCS as it moved southeast from western Kansas late on 10 June to south-central Oklahoma early on 11 June. Smull and Houze (1987) studied its rear-inflow jet structure using single-Doppler data. Biggerstaff and Houze (1991) documented the precipitation and kinematic structure of the mature phase of the squall-line system. Zhang et al. (1989) numerically simulated this MCS using a hydrostatic, mesoscale nested-grid model and Zhang and Gao (1989) and Gao et al. (1990) discussed the simulation in relation to the rear-inflow jet and momentum budget of the storm system, respectively. In addition, Gallus and Johnson (1991) determined the heat and moisture budgets for the squall line using mesonetwork sounding data.

In this section, attention is focused on the surface mesoscale pressure fields associated with this MCS and the wind response to these features. Pressures from the PRE-STORM mesonet have been reduced to 518 m [the average elevation of the National Center for Atmospheric Research (NCAR) Portable Automated Mesonetwork (PAM stations) over Kansas], and tidal effects have been removed following the procedures of Johnson and Hamilton (1988). The 1D time-dependent model is applied to simulate the wind component normal to the squall line. For the 10–11 June squall line, this direction was along 310°–130°. Positive values of this normal component will henceforth be referred to as westerlies and negative values as easterlies. This component of the flow and the horizontal divergence and pressure fields are analyzed using Barnes' (1964) objective analysis scheme.

Of particular interest is the time period from 0100 to 0400 UTC on 11 June, during which the MCS, as well as the mesoscale pressure fields, reached peak intensity. In Fig. 2a, a strong mesohigh can be seen over southwest Kansas at 0100 UTC. The amplitude of the mesohigh was a maximum in that portion of the line where the most intense cells developed prior to 0100 UTC (Johnson and Hamilton 1988). There was also a forward bulging of the squall line in this location, as can be seen from the low-level radar reflectivity from the Wichita, Kansas, WSR-57 radar (Fig. 2a). Ahead of the mesohigh was a presquall mesolow. At this time, a weak area of low pressure was beginning to develop behind the mesohigh where the trailing stratiform re-

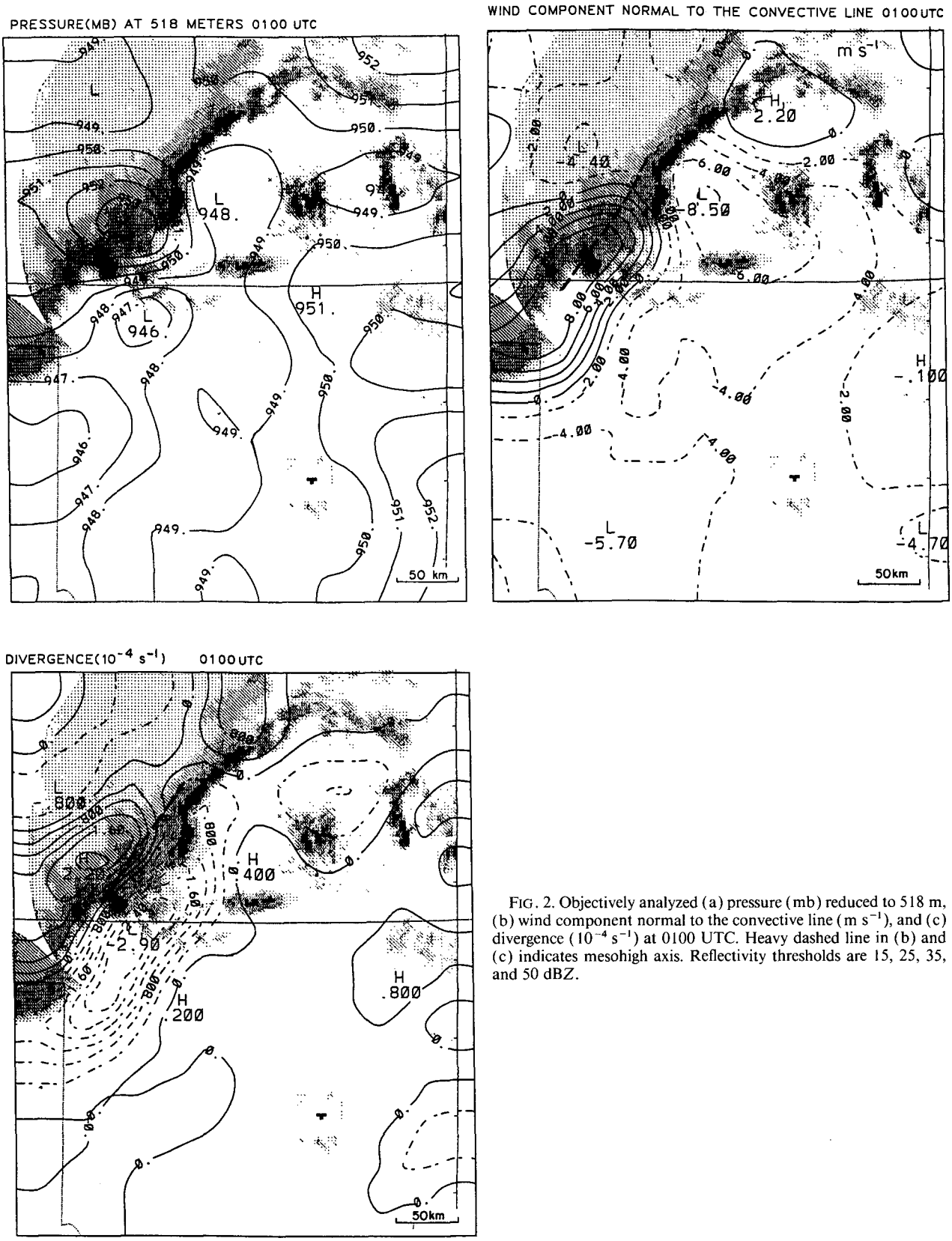

FIG. 2. Objectively analyzed (a) pressure (mb) reduced to 518 m, (b) wind component normal to the convective line (m s^{-1}), and (c) divergence (10^{-4} s^{-1}) at 0100 UTC. Heavy dashed line in (b) and (c) indicates mesohigh axis. Reflectivity thresholds are 15, 25, 35, and 50 dBZ.

gion was forming. Maximum westerlies (ground relative) of ~ 10 m s^{-1} were found along the mesohigh axis (Fig. 2b). Westerlies extended well behind the mesohigh axis, indicating that the instantaneous airflow was directed *forward* through much of this high pressure system. A small area of easterlies was located ~ 50–100 km behind the mesohigh in association with the developing wake low. The divergence field (Fig. 2c) shows that the maximum divergence was occurring ~ 30 km to the rear of the mesohigh axis. Strong convergence extended approximately 100 km ahead of the mesohigh axis. This region of convergence was associated with the leading gust front emanating from the mesohigh, consistent with earlier studies of this storm (Johnson and Hamilton 1988; Biggerstaff and Houze 1991). Finally, an area of weak convergence was located near the developing wake low.

By 0300 UTC, the wake low intensified and became very extensive with a major axis of approximately 200 km (Fig. 3a). In addition, the trailing stratiform region also intensified and became more widespread. Johnson and Hamilton (1988) attribute the rapid development and increased areal coverage of the wake low during this period to the expansion of the stratiform region. During the 2-h period from 0100 to 0300 UTC, the maximum pressure in the mesohigh remained relatively constant. Maximum westerlies reached 13 m s^{-1} just ahead of the mesohigh axis, with a secondary maximum of 8 m s^{-1} to the northeast (Fig. 3b). As at the previous time, westerlies extended behind the mesohigh. The easterlies just ahead of the wake low increased to 7 m s^{-1} as the wake low reached its maximum areal extent, with easterly flow extending ~ 40 km behind the wake-low axis. The divergence to the rear of and the convergence ahead of the mesohigh increased slightly in magnitude by 0300 UTC (Fig. 3c). A pronounced area of convergence was located behind the wake low.

The track of the mesohigh and wake low during the time period of interest is summarized in Fig. 4. The mesohigh moved southeast in association with the leading convective line from southwest Kansas at 0100 UTC to central Oklahoma by 0400 UTC. The wake low, on the other hand, moved east-southeast. While the tracks of these features appear to be independent, they are both related in a complex way to the evolution and propagation of the precipitation regions associated with the squall line. The movement of the mesohigh appears to be primarily dictated by the movement of the convective line and the coldest precipitation downdrafts within it. The movement of the wake low is most likely controlled by the interaction of the rear-inflow jet with the trailing stratiform region and along-line asymmetries in precipitation intensity within it (Johnson and Hamilton 1988; Stumpf et al. 1991). It is evident from Fig. 4 that the squall-line surface pressure field is not strictly one-dimensional; however, it will be shown that the wind response to it can be realistically represented by a model that as a first approximation neglects along-line variations of the flow.

3. Model development

A 1D slab model is used to study the airflow associated with a transient mesoscale pressure wave moving at a constant phase speed. A coordinate system is adopted such that u is the component of the wind normal to the long axis of the mesoscale pressure field (positive in the direction of squall-line motion). Considering a shallow (~ 500 m deep) layer near the earth's surface, the vertically integrated momentum equation can be written to a good approximation as

$$\frac{\partial u_m}{\partial t} = -\frac{1}{\rho}\frac{\partial p_m}{\partial x} - \mathbf{v}_{hm}\cdot\nabla u_m + fv_m + \frac{1}{H}\int_0^H F dz, \quad (1)$$

where $F = -\partial(\overline{u'w'})/\partial z$, the subscript m denotes vertically integrated values, h refers to the horizontal wind components, H represents the depth of the pressure disturbance, an overbar refers to a horizontal average, and a prime refers to the deviation from that average. In (1), the horizontal eddy flux convergences $[-\partial(\overline{u'u'})/\partial x, -\partial(\overline{u'v'}/\partial y]$ are assumed to be small compared with $-\partial(\overline{u'w'})/\partial z$ and are therefore neglected. Vertical advection by the mean flow is small compared with horizontal advection near the earth's surface, and it too is neglected.

As a first approximation, the pressure fields are considered to be quasi-two-dimensional, with much larger momentum advection in the line-normal direction than in the line-parallel direction, that is, $v\partial u/\partial y \ll u\partial u/\partial x$. Also, the Coriolis force fv is neglected since attention will be focused on accelerations over the relatively short 1–2-h period of the development of the mesohigh–wake-low couplet. With these additional assumptions, the momentum equation can now be written (omitting the subscript m) as

$$\frac{\partial u}{\partial t} = -\frac{1}{\rho}\frac{\partial p}{\partial x} - u\frac{\partial u}{\partial x} + \frac{1}{H}\int_0^H F dz, \quad (2)$$

where the friction term is

$$\frac{1}{H}\int_0^H F dz = -\frac{C_D|u|u}{H} - \frac{(\overline{u'w'})}{H}. \quad (3)$$

The first term on the rhs of (3) represents a surface drag, with C_D being the drag coefficient. The second term represents the momentum flux at the top of the model layer. Newton (1950) has shown that in squall-line systems, vertical transport of momentum in convective-scale downdrafts can contribute significantly to the surface winds. This term was neglected in most of the model runs, but it was included in a sensitivity test to assess its relative importance. Results using the full friction equation are discussed in section 8.

As a first approximation, a value for the drag coefficient was found for a statically neutral atmosphere

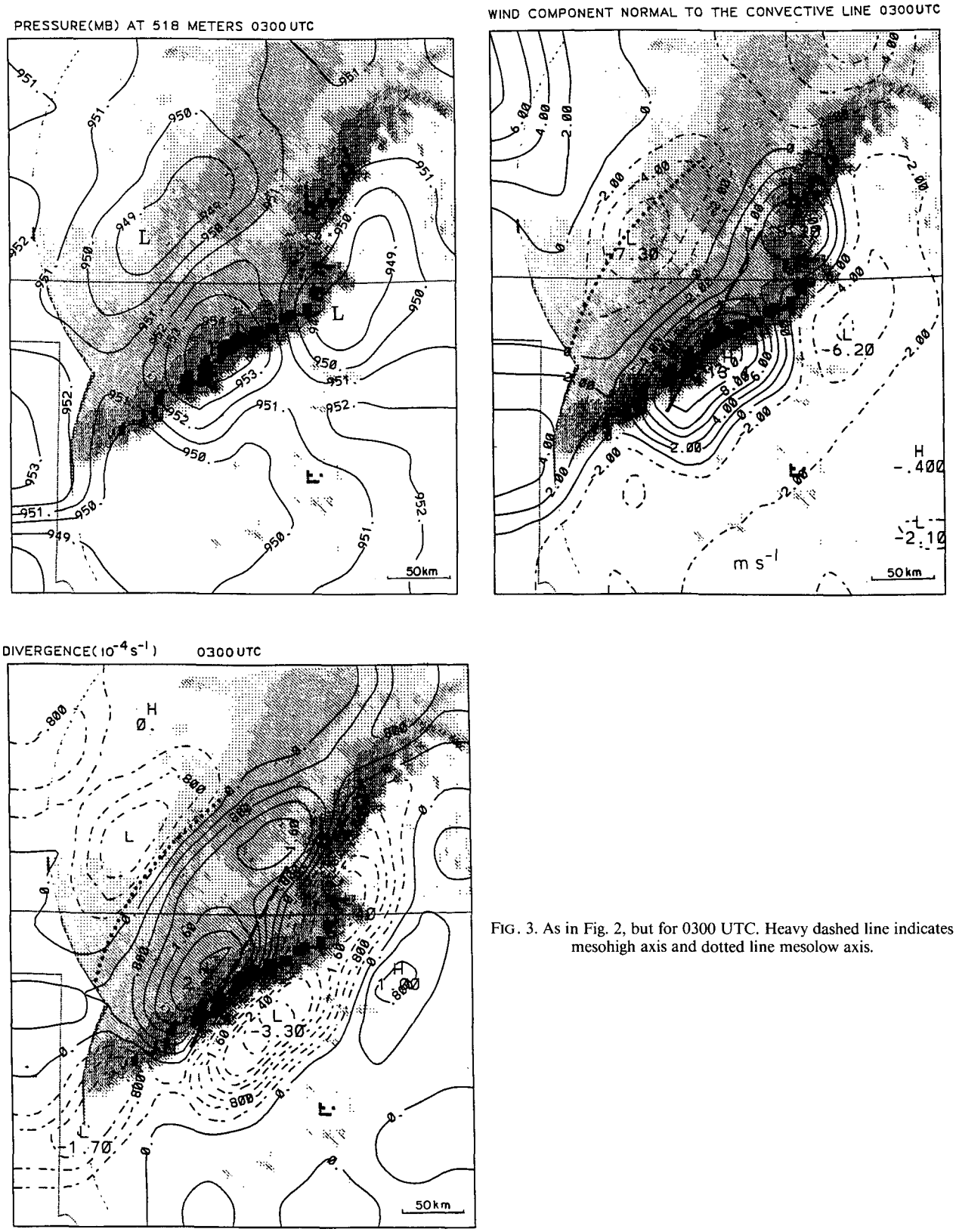

FIG. 3. As in Fig. 2, but for 0300 UTC. Heavy dashed line indicates mesohigh axis and dotted line mesolow axis.

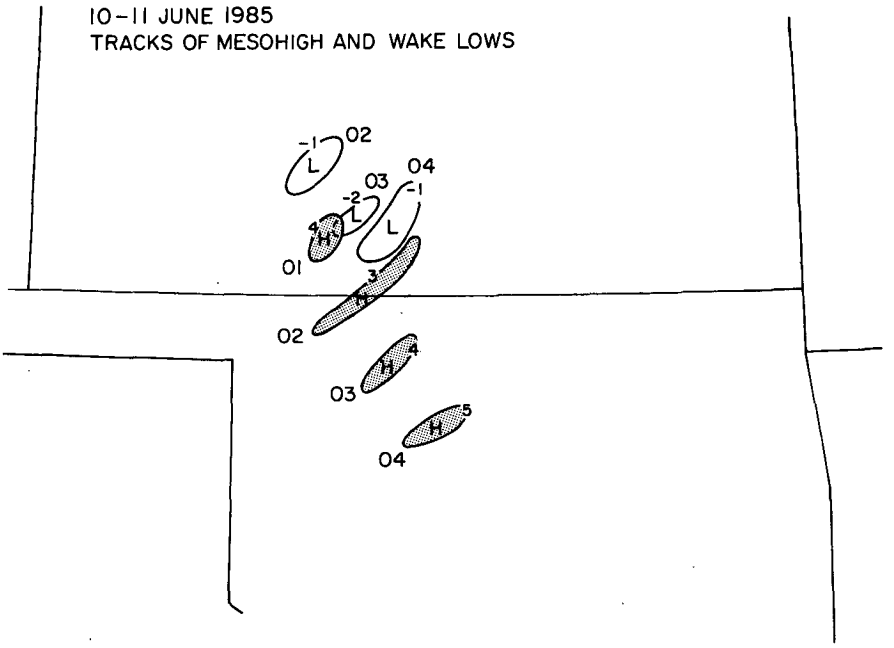

FIG. 4. Tracks of mesohigh and wake low from 0100 to 0400 UTC 11 June 1985. Innermost closed isobars are drawn [labels are departures of pressure (mb) at 518 m from 950 mb].

(C_{DN}) at a height of 10 m. Since the terrain over Oklahoma and Kansas consists primarily of plains, a roughness length z_0 for this type of surface was used. Panofsky and Dutton (1984) give a z_0 of 0.01 m for fairly level grass plains and 0.1 m for farmland, which yields $C_{DN} = 3.35 \times 10^{-3}$ and 7.54×10^{-3}, respectively. A value between these ranges of 5×10^{-3} was used in the model. Actually, conditions behind the convective line were stable, and thus the drag coefficient may be less than what was calculated. For the majority of the model runs, the depth of the pressure disturbance H was assumed to be 500 m. The sensitivity of the results to choices of H and C_D is reported in section 8.

Equation (2) was used to calculate u in the model. It is essentially the same as the equation developed by Garratt and Physick (1983), except that horizontal advection is included but Coriolis effects are omitted. This equation was approximated using a time-centered or leapfrog scheme, as well as a space-centered finite-difference advection scheme of second-order accuracy. Grid (Δx) and time (Δt) spacing used in the model were 5 km and 60 s, respectively. The total domain was 960 km long with a 200-km pressure wave being initialized in the center of the domain. Disturbances of the flow from the wave, which only propagate by advection, do not reach the boundaries over the period of integration. An Asselin (1972) filter was applied at every time step to eliminate the computational mode arising from the leapfrog scheme:

$$u_c^k = u^k + 0.5\nu(u_c^{k-1} - 2u^k + u^{k+1}), \qquad (4)$$

where k is the time index, u_c is the corrected u component, and ν is the filter parameter [set equal to the optimum value of 0.86 recommended by Asselin (1972)]. Results do not vary significantly for values of $\nu > 0.7$. Values in this range appear to be consistent with the recommendations by Schlesinger et al. (1983) based on solutions of the linearized shallow-water equations with diffusive and propagation effects included.

4. Treatment of the pressure field

In Fig. 5, cross sections of the observed adjusted pressure perturbation are displayed in 1-h intervals from 0100 to 0400 UTC 11 June. These cross sections represent the pressure along a line perpendicular to the squall line passing as closely as possible to the centers of the mesohigh and wake low. The mean pressure was determined by averaging the highest pressure in the mesohigh and the lowest pressure in the wake low at each time. Observations indicate that the pressure disturbance had a wavelength of approximately 200 km, especially early in the period, and a roughly sinusoidal shape. Therefore, the pressure wave in the model was chosen to be sinusoidal with a wavelength of 200 km. The observed wave amplitude was somewhat variable, showing a tendency to increase with time, but averaged 2–3 mb. Initial attempts at simulating the wind response to a traveling, constant-amplitude pressure disturbance yielded unstable solutions when starting with a resting base state. Therefore, the amplitude of the

pressure wave in the model was initially set to 0, but then was increased linearly to 2.5 mb at $t = 2$ h. This simulation represents the evolution of the pressure wave of an idealized squall line having perfect symmetry between the mesohigh and wake low, with the results after 2 h corresponding to its mature stage. This assumption is not a true replication of the 10–11 June squall line since the mesohigh development preceded the wake-low development by several hours. Therefore, caution must be exercised in any detailed comparisons with observations from the 10–11 June case.

The phase speed of the pressure wave was determined from the argument that the mesohigh, which is a reflection of the cold pool associated with the thunderstorm downdraft, is a type of density current. The speed of a density current (Seitter 1986) is given by

$$V = k\left(\frac{\Delta p}{\rho_w}\right)^{0.5} + 0.62\bar{U}, \qquad (5)$$

where Δp is the difference in surface pressure between the density current and the environment, ρ_w is the density at the surface in the warm air ahead of the density current, k is a constant, and $\bar{U}$ is the warm-air wind component in the direction of the current motion and is averaged over the depth of the cold pool. To determine the value of k, Seitter applied (5) to 20 gust fronts whose phase speed was known. From these observations, the best value for k is 0.79. Using this value of k, $\Delta p = 6$ mb [the average pressure difference between the axis of the mesohigh and the pressure minima ahead and behind (which constitute the environment for this situation), from Fig. 5], $\bar{U} = -4$ m s^{-1} (estimated from the surface winds in Figs. 2b and 3b), and $\rho_w = 1.2$ kg m^{-3}, a density-current speed of 15.2 m s^{-1} is obtained. This speed is within 1 m s^{-1} of the speeds reported by Johnson and Hamilton (1988) and Rutledge et al. (1988) for the 10–11 June squall line over Kansas and Oklahoma.

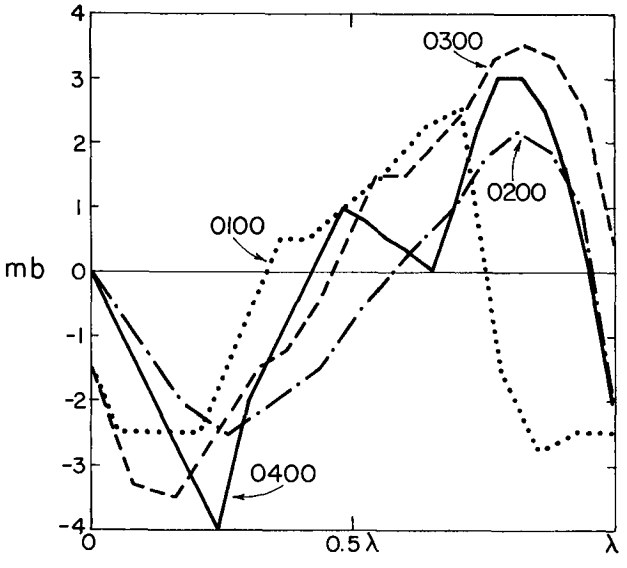

FIG. 5. Pressure variation (mb) across squall line at 0100, 0200, 0300, and 0400 UTC. Average wavelength $\lambda = 200$ km.

Simulations have been carried out for three prescribed maximum pressure amplitudes of the wave: 1.5, 2.5, and 3.5 mb (or peak-to-trough values of 3, 5, and 7 mb). Employing for simplicity an assumption of a resting base state ($\bar{U} = 0$), these amplitudes correspond to associated wave speeds from (5) of 13, 16, and 19 m s^{-1}, respectively. Results from the 16 m s^{-1} wave will be described in greatest detail since they most closely correspond to the observed squall line. The amplitude of the pressure wave was initially set to zero and then increased linearly with every time step until the wave reached its maximum amplitude at $t = 120$ min; however, its phase speed has been assumed to be constant with time in each of the above cases. Although this assumption seems inconsistent with the application of (5) to a growing pressure wave, it is supported by the observations of an approximately constant squall-line speed over the time period of interest and the observation that the mesohigh cold pool developed and became intense very early in the storm history (e.g., Johnson and Hamilton 1988).

5. Model limitations

The purpose of using the highly simplified 1D model developed here is to permit simple interpretation of the relevant physical processes involved in the response of the wind to transient mesoscale pressure fields in squall lines. Many details of the processes, as well as important dynamical interactions between the convective system and the boundary layer, will obviously not be treated by this approach.

A number of model approximations pertain to the treatment of the pressure field.

1) The assumed sinusoidal pressure-wave structure, while reasonable, is an oversimplification. Moreover, effects of the presquall low are not included in the results reported here. (Simulations including a presquall mesolow were conducted but yielded very strong winds ahead of the mesohigh and the solution became unstable. The simplified boundary-layer model used here may not be suitable for the well-mixed layer ahead of the squall line.)

2) The amplitudes of the mesohigh and wake low were assumed identical throughout the model run. Observations show the wake low to develop well after the formation of the mesohigh.

3) The model mesohigh and wake low moved at the same constant speed. The speed was determined by density-current arguments that dictate the movement of the mesohigh. In reality, while the mesohigh moves as a density current, the movement of the wake low is likely controlled by the interaction of the rear-

inflow jet with the stratiform rain area. Specifically, the mesohigh moved steadily southeast with the convective line, while the wake low moved more slowly to the east-southeast and the separation between these two features increased with time (Fig. 4).

4) Finally, the model pressure wave amplified with every time step up until 2 h, whereas during the time period for verification, the observed mesohigh and wake low underwent periods of strengthening *and* weakening.

Other approximations, not related to the pressure field, include the following.

1) The Coriolis force has been neglected. Toward the end of the 2-h model period, Coriolis effects start to become important. The analyses of Johnson and Hamilton (1988) show a relatively strong northerly component of the flow at low levels behind the line, which, after some time, probably contributed to the line-normal component of the flow.

2) A drag coefficient suitable for statically neutral conditions has been assumed. In reality, the atmosphere is statically stable near the surface over most of the squall-line domain. Therefore, the drag coefficient used in the model may have been too large. However, it will be shown that while quantitative differences do exist, the qualitative results do not change for alternative assumptions regarding surface friction.

6. Model results

a. 2.5-mb-amplitude pressure wave

The pressure field and u component at 30, 60, 90, and 120 min for the 2.5-mb wave are shown in Fig. 6. Although the pressure wave is propagating, its position and the ground-relative flow in relation to it are depicted as fixed in Fig. 6 for ease of comparison.

At 30 min, the maximum west wind is slightly less than 1.5 m s^{-1}, with peaks located ~20 km ahead of the mesohigh and ~40 km behind the wake low. A maximum east wind of 1.5 m s^{-1} is found 40 km ahead of the wake low.

Over the next 90-min period, as the pressure wave amplified to 2.5 mb, the west-wind maximum associated with the gust front increased to 11 m s^{-1} while remaining ~20 km ahead of the mesohigh axis. By 120 min, west winds extended 20 km behind the mesohigh. The existence of westerly flow to the west of the mesohigh axis is a result of the propagation of the pressure system. Since the wave is moving eastward faster than all air parcels (throughout the period of integration considered here), all parcels actually move westward relative to the wave. Therefore, eastward-moving air parcels near the mesohigh eventually migrate to the rear of the mesohigh axis where they experience a deceleration and eventually a reversal to westward motion. A similar argument can be made to explain the east winds to the rear of the wake low.

East winds to the rear of the mesohigh also increased to 11 m s^{-1} by 120 min, with the position of the maximum gradually shifting rearward to within 20 km of the wake low at this time. At first glance, it may be somewhat surprising that the maximum easterlies are found ahead of the wake low rather than at the low pressure center. This behavior is explained by considering that the pressure wave is amplifying with time. Two air parcels in the 3.5-mb wave (similar results are obtained with the 2.5-mb wave) were started at the mesohigh axis, one at 20 min and the other at 30 min.

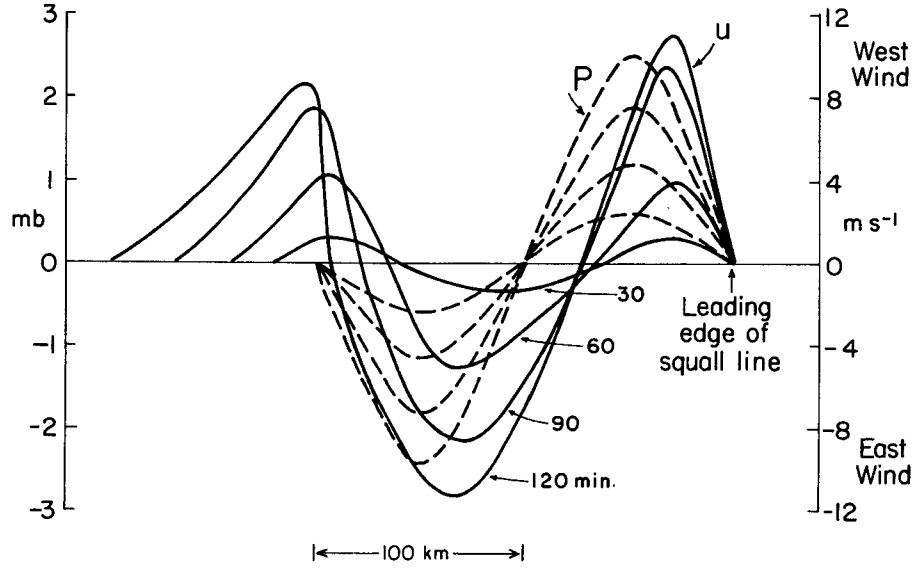

FIG. 6. Predicted wind (m s^{-1}) distributions at 30, 60, 90, and 120 min for 2.5-mb pressure wave.

The first parcel reached the wake low after 70 min, or at $t = 90$ min, with a speed of -9.7 m s^{-1}. At this time, the second parcel was located 17.4 km ahead of the wake low and had a speed of -10.7 m s^{-1}. It later reached a maximum speed of -11.2 m s^{-1} when it came within 2 km of the wake low. The second parcel was able to attain a higher speed than the first, even though it was located well to the east of the wake low, because the pressure wave had amplified by the time it entered the region between the mesohigh and wake low. In support of this explanation, model results at 150 min (not shown), that is, for a 30-min period after steady-state amplitude had been achieved, indicate that the easterly wind maximum and wake-low center had become nearly coincident by that time.

West winds to the rear of the wake low increased to 8 m s^{-1} at 120 min with the crossover from east to west winds shifting rearward with time from near the wake-low axis, initially, to 40 km to its rear at 120 min. The flow pattern at 120 min is consistent with the schematic in Fig. 1. It also resembles the models presented earlier by Fujita (1955) and Pedgley (1962), except in those studies the shift from east to west winds was positioned at the wake-low axis.

The sharp velocity gradients that develop ahead of and behind the mesohigh axis and behind the wake low (Fig. 6) point to the importance of the inclusion of nonlinear advective effects in the model. A scale analysis reveals that the horizontal-advection term often equals or exceeds the pressure-gradient term, particularly at $t > 60$ min in the region ahead of the mesohigh axis.

The variation in divergence across the wave at 30 and 120 min is illustrated in Fig. 7. At 30 min, divergence maxima are 10–20 km behind the mesohigh and 50 km behind the wake low. Convergence maxima are 40 km ahead of the mesohigh along the simulated gust front and 10 km behind the wake low. Over the next 90 min, the same general pattern is observed; however, the amplitudes have increased, the convergence peaks along the gust front and to the rear of the wake low have sharpened, and the phase shifts between the mesohigh–wake-low and trailing divergence–convergence peaks have increased. The increasing phase shifts with time are a result of both the amplification and the propagation of the wave. The convergence behind the wake low at 120 min is particularly strong. Such features may account for the formation of new convection in some instances just behind the wake low (Johnson and Hamilton 1988; Menard et al. 1988; Roux and Ju 1990).

b. Comparison of results for 1.5-, 2.5-, and 3.5-mb-amplitude pressure waves

A comparison of the evolution of the westerlies just behind the gust front for the three different waves is shown in Fig. 8a. The strength of the westerlies is seen to be directly proportional to the wave amplitude, as expected. A similar behavior is seen for the postmesohigh easterlies (Fig. 8b), but for the larger-amplitude waves, the rate of increase with disturbance amplitude is somewhat reduced. This slowing of the easterly wind-speed increase with increasing wave amplitude can be explained by considering air-parcel trajectories. Air parcels were tracked for the 2.5- and 3.5-mb waves from the mesohigh center, starting at $t = 10$ min (where their velocity was zero), until they reached the center of the wake low. The parcel residence times and speeds attained in this region for the 2.5-mb (16 m s^{-1}) and

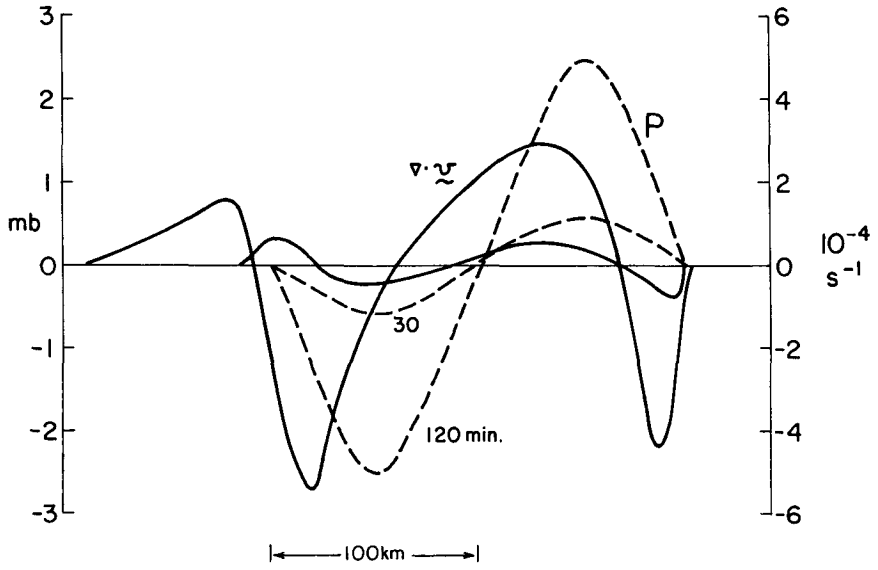

FIG. 7. Predicted divergence (10^{-4} s^{-1}) at 30 and 120 min for 2.5-mb pressure wave.

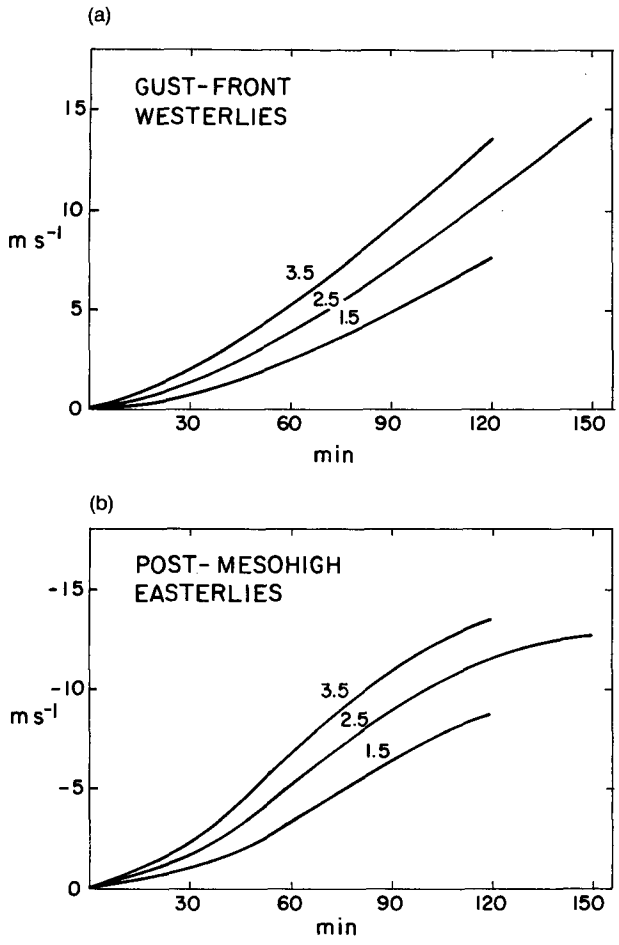

FIG. 8. Predicted (a) gust-front westerlies and (b) postmesohigh easterlies (m s^{-1}) for 1.5, 2.5, and 3.5-mb pressure waves.

3.5-mb (19 m s^{-1}) waves were 84 and 72 min and −8.3 and −8.6 m s^{-1}, respectively. Thus, despite the higher wave amplitude and stronger pressure gradient in the 3.5-mb wave, the easterly speed attained was not much greater due to the shorter residence time between the mesohigh and wake low. This effect is not so apparent in the gust-front westerlies because the air parcels and the wave are moving in the same direction. As higher speeds are attained with stronger waves, residence times in the region of eastward-directed acceleration are not significantly reduced despite the faster speed of the wave.

It is also evident from Fig. 8 that while the gust-front westerly wind speed appears to grow rapidly with time late in the period, the magnitude of the increase in easterly flow levels off. To understand this behavior, two parcels for the 2.5-mb wave were tracked beginning at t = 70 min from two locations: one at the leading edge of the pressure wave (50 km ahead of the mesohigh center) and another from the center of the mesohigh. At t = 150 min, the first parcel had attained a speed of +13.5 m s^{-1} at a distance 11 km ahead of the mesohigh. The second parcel had a speed of −12.6 m s^{-1} at a position 5 km ahead of the wake low. Thus, relative to the wave, the first parcel was displaced only 39 km, whereas the second was displaced 95 km in the same amount of time and was about to exit the region favorable for a westward acceleration. The greater westerly speeds are then a consequence of the fact that parcels located ahead of the mesohigh are moving in the same direction as the pressure wave. These parcels remain in a region favorable for continued acceleration in the same direction longer than those located behind the mesohigh. The latter are moving in the opposite direction of the wave and therefore spend less time in a region of westward acceleration. Consequently, after the wave reaches its full amplitude, the maximum westerlies eventually exceed the maximum easterlies. This effect is not noticed until late in the model run because the pressure gradient ahead of the mesohigh has to be sufficiently strong to allow parcels to gain enough momentum to remain ahead of the high center.

The above analysis explains why hurricane-force winds do not develop in cases where intense pressure gradients exist between the mesohigh and wake low [sometimes equivalent to that observed in the eyewall of a moderate hurricane; e.g., Brunk (1949), Williams (1948, 1953), Johnson et al. (1989), Stumpf et al. (1991)]. The explanation is that air parcels do not remain in the region of intense pressure gradient long enough for high speeds to be attained.

Extending the results from Fig. 8, it can be argued that the maximum westerly wind is limited by the phase speed of the pressure wave. As the speed of an air parcel begins to exceed the phase speed of the pressure wave, the parcel eventually outruns the wave. It then encounters the flat pressure gradient ahead of the mesohigh and decelerates.[1] This type of parcel movement might contribute to the surging motion of many gust fronts. There may be an additional contribution to gust-front surging by vertical momentum transport in the leading convective line. This possibility will be discussed later.[2]

The westerly wind maximum behind the wake low exhibits a different character (Fig. 9a). At 120 min, the strongest west wind is actually achieved for the 1.5-mb wave (although only slightly). To explain this behavior, air parcels were followed through each wave from the center of the wake low at t = 60 min until

[1] Of course, presquall mesolows are often found ahead of the mesohigh (Johnson and Hamilton 1988). In these cases, maximum winds along the gust front may be greater due to the greater distance of a forward-directed pressure gradient between the mesohigh and presquall mesolow.

[2] An additional mechanism for surging at the gust front is the development of pressure perturbations induced by rotational flow about a horizontal axis behind the density-current head (Droegemeier and Wilhelmson 1987).

they reached the flat pressure gradient 50 km to the rear. The initial parcel speeds were −1.6 and −5.0 m s^{-1} in the 1.5- and 3.5-mb pressure waves, respectively. The parcel in the 1.5-mb wave had a residence time of 84 min and reached a speed of 7.4 m s^{-1} upon exiting the wave. The parcel in the 3.5-mb wave had a residence time of only 41 min and reached a speed of only 5.4 m s^{-1}. Both the higher speed of the 3.5-mb wave and stronger easterlies through the wake low contributed to this reduced residence time. Therefore, the 1.5-mb wave contained stronger west winds behind the wake low, despite its smaller amplitude due to a combination of factors contributing to longer residence times for parcels in a region favorable for eastward acceleration. Of course, these conclusions are based on results toward the end of the simulations and, considering the omission of Coriolis and other effects, should be viewed with caution.

The increasing west winds with lower wave amplitude at 120 min also contribute to stronger post–wake-low convergence at that time (Fig. 9b). If real, this finding may have significance for the generation of convection to the rear of squall lines. Johnson and Hamilton (1988) noted that a line of weak convection developed behind the wake low during the 10–11 June event. Sounding data indicated that strong subsidence within the descending rear-inflow jet effectively capped the growth of the convective line. If squall lines with weak wake lows have yet enhanced surface convergence in the wake-low region, then it might be possible for such systems to more readily develop postsquall convection, particularly if there is correspondingly weak descent above the zone of surface convergence. Stumpf and Gallus (1989) noted just this possibility in connection with the development of a new convective line behind the 26–27 June PRE-STORM squall line. Redevelopment of convection was also reported within the wake-low region of an MCS studied by Menard et al. (1988).

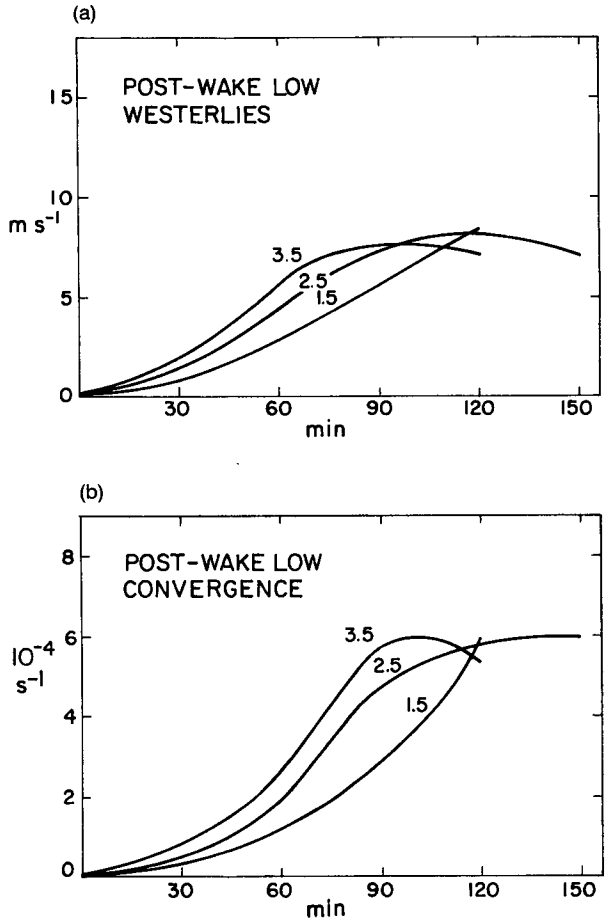

FIG. 9. Predicted (a) post–wake-low westerlies (m s^{-1}) and (b) post–wake-low convergence (10^{-4} s^{-1}) for 1.5-, 2.5-, and 3.5-mb pressure waves.

7. Comparison of model results with observations

Given the earlier-stated limitations of the 1D model, only a qualitative comparison will be made between the model results and the airflow in the 10–11 June squall-line system. Model output from the 2.5-mb (16 m s^{-1}) wave is used since it best resembles the amplitude and speed of the observed pressure wave. Comparison of the model results (Figs. 6 and 7) with observations (Figs. 2 and 3) indicates that both wind and divergence fields were similar once the model pressure wave reached full amplitude, with extremes generally the same order of magnitude. The most significant difference occurred with the convergence to the rear of the wake low where the model results were over three times the observed values. The observations of weaker postmesohigh easterlies and wake-low convergence than that given by the model may be a result of more stable conditions in the wake-low region than in the leading convective line. Soundings taken near the wake low (Fig. 17, Johnson and Hamilton 1988) indicate marked low-level stability and strong low-level wind shears. Therefore, unlike in the leading convective line, vertical mixing is probably inhibited in the vicinity of the wake low, and the surface-measured values of winds and convergences may be an underestimate for the boundary layer as a whole.

The model phase-shift pattern between wind and divergence extrema and mesohigh–wake-low axes (cf. Figs. 2, 3, 6, and 7) was similar to the observed pattern. Both the model and the observations show the following features:

- the maximum westerlies are found ahead of the mesohigh;
- the maximum easterlies are located ahead of the wake low;
- the maximum divergence occurs behind the mesohigh;

• the maximum convergence associated with the wake low occurs behind the low center.

In summary, reasonable agreement is noted between model results and the observations for the 10–11 June squall-line case, despite the model simplicity.

8. Model sensitivity to friction

The maximum westerlies and easterlies (MW and ME) and maximum divergence and convergence (MD and MC) for a given drag coefficient C_D and model layer depth H are shown in Table 1. These values are the maximum values in the grid at $t = 150$ min for a 200-km pressure wave with a maximum amplitude of 2.5 mb.

When C_D is held constant at 0.005 and H is increased from 500 to 1000 m, the increases in MW, ME, MD, and MC are 12%, 6%, 9%, and 13%, respectively. When H is held constant at 500 m and C_D is decreased from 0.005 to 0.001, MW, ME, MD, and MC increase by 22%, 10%, 11%, and 63%, respectively. In the absence of any friction, MW, ME, MD, and MC are increased over the standard model run by 30%, 13%, 34%, and 100%, respectively.

It appears that convergence is most sensitive to changes in the magnitude of the friction term. By 150 min, the position of this maximum convergence is shifted to the simulated gust front ahead of the mesohigh, rather than behind the wake low. The large sensitivity of MC to friction is due to an increasing gradient of u along the gust front as friction is reduced. The wind speed just behind the gust front increases with decreasing friction. But several kilometers ahead of the gust front, where the pressure gradient is flat, the wind remains calm, thereby sharply increasing convergence in this region.

The increase in wind speed when friction is reduced can lead to hazardous high-wind conditions over open ocean areas. Such a situation was documented by Ely (1982) along the Texas gulf coast in 1981. In this instance, strong winds developed between the mesohigh and wake low of a squall-line system as it moved over open water, which significantly affected boating, fishing, and oil operations in the area.

TABLE 1. Sensitivity of wind and divergence maxima to friction, as determined by various values of the drag coefficient C_D and boundary-layer depth H (m). Values listed are at 150 min for the 2.5-mb wave.

Friction	Westerly maximum ($m\ s^{-1}$)	Easterly maximum ($m\ s^{-1}$)	Maximum divergence ($10^{-4}\ s^{-1}$)	Maximum convergence ($10^{-4}\ s^{-1}$)
$C_D = 0.005$ $H = 500$ m	14.6	−12.6	3.5	6.0
$C_D = 0.005$ $H = 700$ m	15.5	−13.0	3.7	6.4
$C_D = 0.005$ $H = 1000$ m	16.4	−13.4	3.8	6.8
$C_D = 0.003$ $H = 500$ m	15.9	−13.2	3.7	6.5
$C_D = 0.001$ $H = 500$ m	17.8	−13.9	3.9	9.8
No friction	19.0	−14.3	4.7	12.0

Up to this point, momentum fluxes at the top of the model layer [second term on rhs of (3)] have been neglected. However, such fluxes may be important in the region of the convective line where convective-scale updrafts and downdrafts are occurring. For this reason, the momentum-transport term, $\overline{u'w'}$, was applied to the first quarter-wavelength of the pressure wave (which is analogous to the region of the convective line). The value for $\overline{u'w'}$ was taken from LeMone et al. (1984). They found a $\overline{u'w'} = -0.8\ m^2\ s^{-2}$ at 500 m for a tropical MCS moving at 14 $m\ s^{-1}$. The value from LeMone et al. (1984) is normalized to a 100-km flight-leg length and may be less than that appropriate for the 50-km quarter-wavelength considered here. Despite uncertainties in this estimate, the above value should provide a reasonable measure of the sensitivity of the results to the inclusion of the vertical transport of momentum.

The inclusion of momentum transport altered the wind flow near the mesohigh (Fig. 10a). Since $\overline{u'w'}$ is negative, momentum transport caused an increase in westerly winds at the surface. This is reflected by a maximum west wind of 14.9 $m\ s^{-1}$ when momentum transport was included, as opposed to 10.9 $m\ s^{-1}$ (from Fig. 6) when it was not (a 37% increase). As a result, convergence ahead of the mesohigh increased from 4.3 $\times\ 10^{-4}$ (Fig. 7) to 6.3 $\times\ 10^{-4}\ s^{-1}$ (Fig. 10b). Also, divergence to the rear of the mesohigh increased from 3.2 to 3.9 $\times\ 10^{-4}\ s^{-1}$, since to the rear of the mesohigh $\overline{u'w'} = 0$, and hence the westerly acceleration in that region due to momentum transport is assumed to be zero.

As far as phase relationships are concerned, when momentum transport was included, the maximum west wind and convergence were located 5 km ahead of their positions when momentum transport was not considered. The maximum divergence was shifted ahead 15 km to within 8 km of the mesohigh axis.

In summary, momentum transport by convective-scale updrafts and downdrafts, assuming values given by LeMone et al. (1984), can significantly enhance the westerly flow and convergence along the gust front. Nonsteadiness in such transport, associated with the life cycle of cells along the leading convective line, could contribute to surging along the gust front. Behind the convective line, this effect is presumed to be minimized due to the high stability of the rain-cooled air.

9. Summary

A simple, 1D slab model has been developed to simulate the wind response to transient mesoscale pressure fields that often accompany midlatitude squall lines. Aspects of the model, such as the treatment of friction, are patterned after Garratt and Physick (1983); however, in our study, we included the effects of nonlinear advection while omitting Coriolis effects. The line-

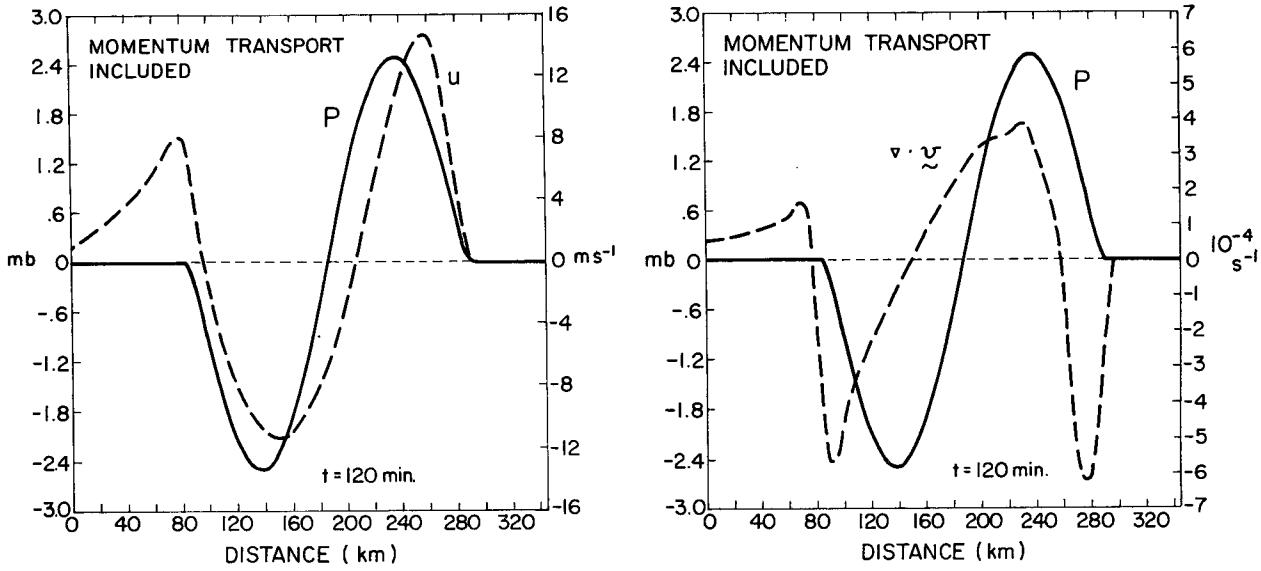

FIG. 10. Predicted (a) wind distribution (m s^{-1}) and (b) divergence (10^{-4} s^{-1}) at 120 min for 2.5-mb pressure wave with effects of convective-line momentum transport at model-layer top included.

normal component of the flow is predicted, while the line-parallel component is considered negligible in comparison. To represent the mesohigh–wake-low couplet, we assume a simple sinusoidal pressure wave with constant wavelength propagating at a constant phase speed through a uniform environmental pressure. The phase speed of the wave was determined by the assumption that it moved as a density current. Thus, the phase speed of the wave was proportional to the square root of its pressure amplitude (Seitter 1986). The amplitude of the pressure wave was initially zero but then increased linearly with time to a maximum amplitude at t = 120 min. This gradual buildup of the pressure amplitude was necessary to prevent instabilities from occurring in the model-derived wind field.

Model results agree reasonably well with the schematic displayed in Fig. 1. In the simulated wind field, the instantaneous airflow was directed forward through the mesohigh and rearward through the wake low. Nonlinear advective effects are important in the evolution of the flow. An axis of divergence was located behind the mesohigh, with convergence occurring ahead of the mesohigh along the gust front and at the back edge of the wake low. The model was run using pressure waves with various maximum amplitudes (hence, various phase speeds). Regardless of the wave amplitude, the wind field was similar to that depicted in Fig. 1.

Model results verify that the existence of westerly flow to the west of the mesohigh axis and easterly flow to the west of the wake low are a result of the propagation of the pressure systems. Since the wave is moving eastward faster than the air parcels (throughout the period of integration), all parcels actually move westward relative to the wave. Therefore, eastward-moving air parcels near the mesohigh eventually migrate to the rear of the mesohigh axis where they experience a deceleration and eventually a reversal to westward motion. A similar argument can be made to explain the east winds behind the wake low.

Through 2.5 h of integration, the west winds behind the gust front increase more rapidly with time than the east winds between the mesohigh and wake low. This behavior is explained by noting that the residence times for air parcels just behind the gust front are much longer than those for parcels to the rear of the mesohigh. Thus, the gust-front westerlies can build up to values reaching and exceeding the speed of the wave, thereby exhibiting a pulsing behavior, perhaps contributing to the surging behavior of gust fronts. The shorter residence times of parcels behind the mesohigh explains why hurricane-force winds are not observed there on occasions when extremely intense pressure gradients exist between the mesohigh and wake low.

A somewhat surprising result from comparing 1.5-, 2.5-, and 3.5-mb wave-amplitude simulations at 120 min was that west winds, observed to the rear of the wake low, were strongest in the weakest (1.5-mb) wave. Analysis of air-parcel trajectories showed that the slower movement of the 1.5-mb wave allowed for higher parcel residence time in a region favorable for eastward acceleration. The higher residence time permitted stronger post–wake-low west winds in this wave, despite the lower pressure amplitude. This effect also contributed to stronger convergence behind the wake low in this case. This finding may be of possible significance for the generation of new convection behind slow-moving squall lines (Johnson and Hamilton 1988; Menard et al. 1988; Stumpf and Gallus 1989).

Model results are mildly sensitive to assumptions regarding the strength of surface friction, except that convergence along the leading gust front is significantly

enhanced as friction is reduced. This behavior is a result increased wind speeds behind the gust front encountering calm winds in the assumed flat pressure gradient ahead of the wave. Reduced friction over oceans may contribute to enhanced wind speeds within squall lines occurring in marine environments, as has been observed in the intense pressure gradient between the mesohigh and wake low (Ely 1982). The inclusion of momentum transports within the leading convective line (following LeMone et al. 1984) yields a marked increase in the winds and convergence along the leading gust front.

Model results compare reasonably well with observations of the wind field near the mesohigh and wake low of an intense squall line that moved through Kansas and Oklahoma on 10–11 June 1985. Both the model and the observations showed that the maximum westerlies occurred ahead of the mesohigh, maximum easterlies were found ahead of the wake low, maximum divergence occurred behind the mesohigh, and convergence maxima were located both just behind the gust front and to the rear of the wake low.

An obvious improvement of the model developed here would be the addition of the Coriolis force, thereby allowing for longer time integrations and including the effects of line-parallel motion. Furthermore, the addition of resolution within the boundary layer could perhaps assist in a better understanding of the observations of vertical wind shears in these systems.

Acknowledgments. The helpful comments of Prof. Wayne Schubert and two anonymous reviewers are appreciated. This research has been supported by the National Science Foundation under Grant ATM-8711649 and by the National Oceanic and Atmospheric Administration through Cooperative Institute for Research in the Atmosphere (CIRA) at Colorado State University (CSU) under Grant NA 85 RAH 05045.

REFERENCES

Asselin, R., 1972: Frequency filter for time integration. *Mon. Wea. Rev.*, **100,** 487–490.

Barnes, S. L., 1964: A technique for maximizing details in numerical weather map analysis. *J. Appl. Meteor.*, **3,** 396–409.

Biggerstaff, M. I., and R. A. Houze, Jr., 1991: Kinematic and precipitation structure of the 10–11 June 1985 squall line. *Mon. Wea. Rev.*, **119,** 3034–3065.

Brunk, I. W., 1949: The pressure pulsation of 1 April 1944. *J. Meteor.*, **6,** 181–187.

——, 1953: Squall lines. *Bull. Amer. Meteor. Soc.*, **34,** 1–9.

Droegemeier, K. K., and R. B. Wilhelmson, 1987: Numerical simulation of thunderstorm outflow dynamics. Part I: Outflow sensitivity experiments and turbulence dynamics. *J. Atmos. Sci.*, **44,** 1180–1210.

Ely, G. F., 1982: Case study of a significant thunderstorm wake depression along the Texas coast: May 29–30 1981. NOAA Tech. Memo. NWS SR-105, 64 pp.

Fujita, T. T., 1955: Results of detailed synoptic studies of squall lines. *Tellus,* **7,** 405–436.

Gallus, W. A., Jr., and R. H. Johnson, 1991: Heat and moisture budgets of an intense midlatitude squall line. *J. Atmos. Sci.*, **48,** 122–146.

Gao, K., D.-L. Zhang, M. W. Moncrieff, and H.-R. Cho, 1990: Mesoscale momentum budget in a midlatitude squall line: A numerical case study. *Mon. Wea. Rev.*, **118,** 1011–1028.

Garratt, J. R., and W. L. Physick, 1983: Low-level wind response to mesoscale pressure systems. *Bound.-Layer Meteor.*, **27,** 69–87.

Green, J. L., 1989: Analysis of surface pressure features during an episode of mesoscale convective systems. M.S. thesis, Texas Tech University, 75 pp. [Available from Prof. Colleen Leary, Atmospheric Science Group, Texas Tech University, Lubbock, TX 79409.]

Johnson, R. H., and P. J. Hamilton, 1988: The relationship of surface pressure features to the precipitation and air flow structure of an intense midlatitude squall line. *Mon. Wea. Rev.*, **116,** 1444–1472.

——, S. Chen, and J. J. Toth, 1989: Circulations associated with a mature-to-decaying mesoscale convective system. Part I: Surface features—Heat bursts and mesolow development. *Mon. Wea. Rev.*, **117,** 942–959.

LeMone, M. A., G. A. Barnes, and E. J. Zipser, 1984: Momentum flux by lines of cumulonimbus over the tropical oceans. *J. Atmos. Sci.*, **41,** 1914–1932.

Mahrt, L. J., 1974: Time-dependent, integrated planetary boundary layer flow. *J. Atmos. Sci.*, **31,** 457–464.

Menard, R. D., D. L. Sims, and J. M. Fritsch, 1988: Case example of the effect of a wake low on subsequent convective events. Preprints, *15th Conf. on Severe Local Storms,* Amer. Meteor. Soc., Baltimore, 225–228.

Newton, C. W., 1950: Structure and mechanisms of the pre-frontal squall line. *J. Meteor.*, **10,** 210–222.

Panofsky, H. A., and J. A. Dutton, 1984: *Atmospheric Turbulence.* John Wiley & Sons, 397 pp.

Pedgley, D. E., 1962: A meso-synoptic analysis of the thunderstorms on 28 August 1958. *Brit. Meteor. Off., Geophys. Mem.*, No. 106, 74 pp.

Roux, F., and S. Ju, 1990: Single-Doppler observations of a West African squall line on 27–28 May 1981 during COPT 81: Kinematics, thermodynamics, and water budget. *Mon. Wea. Rev.*, **118,** 1826–1854.

Rutledge, S. A., R. A. Houze, Jr., M. I. Biggerstaff, and T. Matejka, 1988: The Oklahoma-Kansas mesoscale convective system of 10–11 June 1985: Precipitation structure and single-Doppler radar analysis. *Mon. Wea. Rev.*, **116,** 1409–1430.

Schlesinger, R. E., L. W. Uccellini, and D. R. Johnson, 1983: The effects of the Asselin time filter on numerical solutions to the linearized shallow-water wave equations. *Mon. Wea. Rev.*, **111,** 455–467.

Seitter, K. L., 1986: A numerical study of atmospheric density current motion including the effects of condensation. *J. Atmos. Sci.*, **43,** 3068–3076.

Smull, B. F., and R. A. Houze, Jr., 1987: Rear inflow in squall lines with trailing stratiform precipitation. *Mon. Wea. Rev.*, **115,** 2869–2889.

Stumpf, G. J., and W. A. Gallus, Jr., 1989: An examination of new convective development with a PRE-STORM squall line case. Preprints, *24th Conf. on Radar Meteorology,* Amer. Meteor. Soc., Tallahassee, 506–509.

——, R. H. Johnson, and B. F. Smull, 1991: The wake low in a midlatitude mesoscale convective system having complex convective organization. *Mon. Wea. Rev.*, **119,** 134–158.

Williams, D. T., 1948: A surface micro-study of squall-line thunderstorms. *Mon. Wea. Rev.*, **76,** 239–246.

——, 1953: Pressure wave observations in the central Midwest, 1952. *Mon. Wea. Rev.*, **81,** 278–298.

——, 1954: A surface study of a depression-type pressure wave. *Mon. Wea. Rev.*, **82,** 289–295.

Zhang, D.-L., and K. Gao, 1989: Numerical simulation of an intense squall line during 10–11 June 1985 PRE-STORM. Part II: Rear inflow, surface pressure perturbations, and stratiform precipitation. *Mon. Wea. Rev.*, **117,** 2067–2094.

——, ——, and D. B. Parsons, 1989: Numerical simulation of an intense squall line during 10–11 June 1985 PRE-STORM. Part I: Model verification. *Mon. Wea. Rev.*, **117,** 960–994.